Molecular dynamics of branched hexaalkyl hexa-*peri*-hexabenzocoronenes

2008 J. Phys.: Condens. Matter 20 244105

(http://iopscience.iop.org/0953-8984/20/24/244105)

J. Phys.: Condens. Matter **20** (2008) 244105 (6pp) doi:10.1088/0953-8984/20/24/244105

Molecular dynamics of branched hexaalkyl hexa-*peri*-hexabenzocoronenes

M M Elmahdy[1,2], G Floudas[1,2], M Kastler[3] and K Müllen[3]

[1] Department of Physics, University of Ioannina, 451 10 Ioannina, Greece
[2] Foundation for Research and Technology-Hellas (FORTH), Biomedical Research Institute (BRI), Greece
[3] Max-Planck Institute for Polymer Research, 55128 Mainz, Germany

E-mail: gfloudas@cc.uoi.gr (G Floudas)

Received 3 March 2008
Published 29 May 2008
Online at stacks.iop.org/JPhysCM/20/244105

Abstract

The molecular dynamics of discotic liquid crystalline hexa-*peri*-hexabenzocoronenes (HBC-$C_{10,6}$ and HBC-$C_{14,10}$) with long alkyl side chains branched in close vicinity to the HBC aromatic core were studied by dielectric spectroscopy. The two compounds display a weak dipolar relaxation (α-process) manifested by a Vogel–Fulcher–Tammann (VFT) dependence and have almost the same glass temperature ($\sim$215 K) in excellent agreement with the value from differential scanning calorimetry. The origin of this process is the freezing of the in-plane disc rotation. Controlled experiments revealed that the weak dipole moment associated with the α-process is due to oxidation.

(Some figures in this article are in colour only in the electronic version)

1. Introduction

In the past two decades, discotic liquid crystals have attracted considerable interest because of their unique self-organization behavior into columnar superstructures, leading to high charge carrier mobilities along the columnar stacks [1]. This feature resulted in a successful application of such materials in field-effect transistors and photovoltaic devices [2]. Hexa-*peri*-hexabenzocoronenes (HBCs) are particularly promising because their large aromatic core permits one of the highest values for the intrinsic charge carrier mobility [3–5]. The non-substituted HBCs do not reveal any phase behavior or solubility [6], therefore the attachment of flexible aliphatic chains to the HBCs periphery, as depicted in scheme 1, is an elegant tool to introduce solubility and thus processability [7, 8]. These are the three major phases found in most discotic HBCs: crystalline, liquid crystalline and isotropic [9]. In the crystalline state, the disc-shaped molecules organize into columns that further assemble into a two-dimensional lattice composed of nanophase separated tilted aromatic cores and more flexible alkyl chains. Within the crystalline state, discs possess some mobility, thus this phase is better described as columnar plastic crystalline (Col_p). In the columnar liquid crystalline phase, the discs rotate freely around the columnar axis. In the isotropic phase, the columnar structures break into monomeric species, leading to an amorphous melt.

Molecular dynamics of discotic liquid crystals have been studied by different techniques such as dielectric spectroscopy (DS) [10–14], nuclear magnetic resonance (NMR) [5, 9, 15], neutron scattering [16–18] and computer simulations [19] to probe the molecular dynamics of the aromatic core as well as the hydrocarbon side chains. Since glass formation is generally attributed to the freezing of disordered matter, the observation of glass transition dynamics in the highly ordered plastic crystal phase of triphenylene-based compounds was a rather spectacular finding [14, 20–22]. ^{2}H NMR and dielectric spectroscopy studies on triphenylene derivatives revealed that the glass transition is related to the rotation of the discs around their columnar axis and is not coupled with the side chain mobility [12, 15, 23, 24]. In another hexasubstituted triphenylene derivative, where one of the side chains is a chloroester, it was found that the glass transition in columnar phases may be anisotropic both with respect to dynamic and thermodynamic considerations [10].

Herein, we employ the two HBCs with the highest charge carrier mobilities and investigate the molecular dynamics by dielectric spectroscopy (DS) within the different phases. An ultimate goal of such studies is to understand how the local (and perhaps global) disc dynamics within the columns

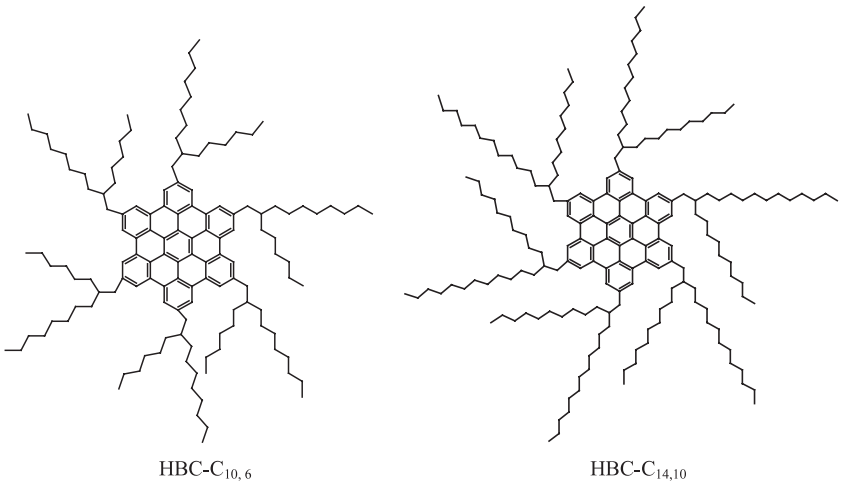

Scheme 1. Schematic representation of the HBC-$C_{10,6}$ (left) and HBC-$C_{14,10}$ (right).

influence the charge carrier mobility. Because of molecular symmetry, a strong dielectrically active process is not expected in these compounds. Nevertheless, we find a very weak dipolar relaxation with a non-Arrhenius temperature-dependence that freezes at 215 K. The origin of this process is discussed in terms of the freezing of the in-plane disc rotation at the respective glass temperature (T_g).

2. Materials and methods

2.1. Samples

Scheme 1 shows the chemical structure of the investigated molecules. The synthesis of the HBC-$C_{14,10}$ and HBC-$C_{10,6}$ has been reported earlier [8].

2.2. Differential scanning calorimetry (DSC)

A Mettler Toledo Star DSC was used with a heating and cooling rate of 10 K min^{-1}. In figure 1, the second heating and cooling runs are shown for the HBC-$C_{10,6}$. A clear step in the specific heat can be seen at the glass temperature (T_g) with a value of 220 K, followed by two endothermic peaks at 290 and 370 K. In figure 2, the DSC trace for the HBC-$C_{14,10}$ during the second heating and cooling runs shows an endothermic peak at 321 K (on heating). The transition temperatures, heats of fusion and respective phases of HBC-$C_{14,10}$ and HBC-$C_{10,6,}$ obtained during the second heating and cooling runs, are compiled in table 1.

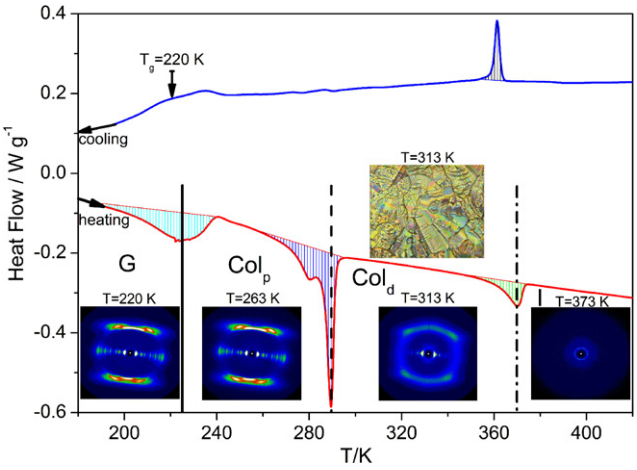

Figure 1. DSC trace of the HBC-$C_{10,6}$ obtained during the second cooling and heating runs with a rate of 10 K min^{-1}. The vertical arrow indicates the glass temperature. The vertical solid, dashed and dash–dotted lines give the locations of the transition temperatures from the glassy state (G) to the columnar plastic crystalline phase (Col_p) (solid line). to the columnar disordered LC phase (Col_d) (dashed line). and to the isotropic phase (I) (dash–dotted line). 2D-WAXS images obtained from an oriented fiber (T_{extr} = 253 K) are shown at four temperatures corresponding to the glassy state (220 K), Col_p phase (263 K), Col_d phase (313 K), and to the I phase (373 K). A polarizing optical microscopy (POM) image of the HBC-$C_{10,6}$ sandwiched between two glass slides and cooled at 0.1 K min^{-1} is shown. The image was taken at 313 K (i.e. within the Col_d phase) and suggests a smectic mesophase.

2.3. Polarizing optical microscopy (POM)

A Zeiss Axioskop 40 POM with a Linkam THMS600 heating/cooling stage was used to identify the types of mesophases. The Linkam THMS600 stage had a temperature range of 77–873 K with temperature stability of 0.1 K. Sample preparation involved placing a small amount between two glass slides then mounted on a 0.17 mm cover slip on a highly polished silver heating element that ensured high heat transfer. A platinum resistor sensor, accurate to 0.01 K, provided an accurate and stable temperature signal. An LNP94/2 liquid nitrogen pump cooling system enabled controlled cooling rates as fast as 130 K min^{-1}. The samples were heated to the isotropic phase then slowly cooled to the desired temperatures with cooling rates of 0.1 K min^{-1}. Some representative images are included in figures 1 and 2. The images display a spherulitic morphology for HBC-$C_{14,10}$ with a radial columnar orientation and a 'scale-like' texture of the HBC-$C_{10,6}$ with columnar growth around the nucleation center [25, 26].

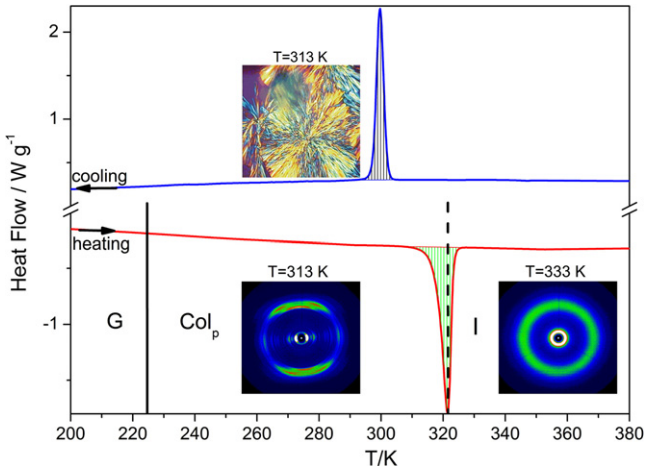

Figure 2. DSC trace of the HBC-$C_{14,10}$ obtained during the second cooling and heating runs with a rate of 10 K min^{-1}. Upon heating the HBC-$C_{14,10}$ exhibits one phase transition at 321 K (300 K on cooling) from the columnar plastic crystalline (Col_p) to the isotropic phase (I). 2D-WAXS images obtained from an extruded fiber (T_{extr} = 298 K) are shown at two temperatures corresponding to the columnar plastic crystalline phase (313 K) and to the isotropic phase (333 K). POM image of the HBC-$C_{14,10}$ sandwiched between two glass slides cooled at 0.1 K min^{-1} is shown at 313 K, i.e. within the Col_p phase. This image shows the formation of regular spherulites.

2.4. Wide-angle x-ray scattering (WAXS)

The two-dimensional-WAXS (2D-WAXS) experiments were performed by using the x-ray beam with pinhole collimation and a 2D detector (Siemens A102647) with 1024 × 1024 pixels. A double graphite monochromator for the Cu Kα radiation (λ = 0.154 nm) was used. Measurements were made from macroscopically oriented cylindrical filaments with a diameter of 0.7 mm. All patterns were recorded with a vertical orientation of the filament axis and the x-ray beam perpendicular to the filament. Some typical patterns are included in figures 1 and 2 for the HBC-$C_{10,6}$ and HBC-$C_{14,10}$, respectively.

2.5. Dielectric spectroscopy

The sample cell consisted of two electrodes 20 mm in diameter and the sample with a thickness of 50 μm maintained by Teflon spacers. The dielectric measurements were made at different temperatures in the range from 173 to 373 K, at atmospheric pressure, and for frequencies in the range from 1×10^{-2} to 1×10^{6} Hz, using a Novocontrol BDS system composed of a frequency response analyzer (Solartron Schlumberger FRA 1260) and a broadband dielectric converter. The complex dielectric permittivity $\varepsilon^* = \varepsilon' - \mathrm{i}\varepsilon''$, where ε' is the real and ε'' is the imaginary part, is a function of frequency ω, temperature T, and pressure P, $\varepsilon^* = \varepsilon^*(\omega, T, P)$ [27]. In the analysis of the DS spectra, we have used the empirical equation of Havriliak and Negami (HN):

$$\varepsilon^*(T, P, \omega) = \varepsilon_\infty(T, P) + \frac{\Delta\varepsilon\,(T, P)}{\left[1 + (\mathrm{i}\omega\tau_{\mathrm{HN}}\,(T, P))^{\alpha}\right]^{\gamma}} + \frac{\sigma_0\,(T, P)}{\mathrm{i}\varepsilon_f\omega} \quad (1)$$

Table 1. Thermal characterization and phase transitions of the investigated HBCs. (Note: G^a: glass transition from DSC, G^b: glass transition from DS, Col_p: columnar plastic crystalline phase, Col_d: columnar disordered LC phase, I: isotropic phase, ^{c}: from DS. Parentheses indicate values during cooling.)

Compound	Transition temperature (K)	Enthalpy (J g^{-1})	Phase transition
HBC-$C_{10,6}$	220	—	G^a
	290 (258)^c	9.3	$Col_p \rightarrow Col_d$
	370 (362)	2.5 (2.8)	$Col_d \rightarrow$ I
	217	—	G^b
HBC-$C_{14,10}$	321 (300)	35.7 (34.4)	$Col_p \rightarrow$ I
	215	—	G^b

where $\varepsilon_\infty(T, P)$ is the high frequency permittivity, $\tau_{\mathrm{HN}}(T, P)$ is the characteristic relaxation time in this equation, $\Delta\varepsilon(T, P) = \varepsilon_0(T, P) - \varepsilon_\infty(T, P)$ is the relaxation strength, α, γ (with limits $0 < \alpha$, $\alpha\gamma \leqslant 1$) describe, respectively, the symmetrical and asymmetrical broadening of the distribution of relaxation times, σ_0 is the dc-conductivity and ε_f is the permittivity of free space. From τ_{HN}, the relaxation time at maximum loss, $\tau_{\max}$, is obtained analytically following

$$\tau_{\max} = \tau_{\mathrm{HN}}\left[\frac{\sin\left(\frac{\pi\alpha}{2+2\gamma}\right)}{\sin\left(\frac{\pi\alpha\gamma}{2+2\gamma}\right)}\right]^{-1/\alpha}. \quad (2)$$

The conductivity, $\sigma^*(\omega)$, and the electric modulus, $M^*(\omega)$, are related with the dielectric function $\varepsilon^*(\omega)$ through [28]

$$\sigma^*(\omega) = \mathrm{i}\omega\varepsilon_0\varepsilon^*(\omega) = \sigma' + \mathrm{i}\sigma''$$
$$M^*(\omega) = \frac{1}{\varepsilon^*(\omega)} = M' + \mathrm{i}M'' \quad (3)$$

where σ' and σ'' are the real and imaginary parts of the conductivity, and M' and M'' are the real and imaginary parts of the electric modulus, respectively. The electric modulus representation (i.e. the decay of the electric field under conditions of constant dielectric displacement, D) rather than the dielectric function (constant electric field, E) have been proposed not only for systems containing a substantial concentration of mobile carriers but also for any dielectrically active process [27]. This representation can also be used to extract the ionic mobility from the crossing of the real (M') and the imaginary parts (M'').

3. Results and discussion

3.1. Structure

As shown in the DSC trace of the HBC-$C_{10,6}$ (figure 1) a clear step in the specific heat can be seen in the second heating run at the glass temperature (T_g) with a value of about 220 K. T_g is followed by two thermally induced phase transformations at 290 and 370 K. The low temperature transition (290 K) has been discussed as a transition from the columnar plastic crystalline phase (Col_p) to the columnar disordered LC phase

(Col_d). The high temperature transition (370 K) reflects the transformation from the Col_d phase to the isotropic phase (I). The Col_p phase is characterized by three-dimensional (3D) crystal-like order in a hexagonal lattice, while the discs within the columns are able to rotate about the columnar axis. In addition, they show a plastic deformation at room temperature in comparison to crystalline materials [5]. The Col_d phase is characterized by structural disorder such as non-parallel arrangement of the discs, and longitudinal and lateral displacements with free rotation around the columnar axis [29]. We mention here that de Gennes suggested that regions of high and low packing density (the pinched regions) are required to mitigate the packing frustration imposed by the flexible alkyl chains and the rigid cores [30]. On the other hand the HBC-$C_{14,10}$ (figure 2) undergoes a phase transformation directly from the columnar plastic crystalline to the isotropic state at 321 K (on heating). Notice that the glass temperatures of the two compounds are very close, in excellent agreement with the one obtained from the dielectric spectroscopy measurements that will be discussed below. Steric demand at the core periphery lowers the temperature of the isotropic phase to 370 and 321 K for the HBC-$C_{10,6}$ and HBC-$C_{14,10}$, respectively.

POM images of the HBC-$C_{10,6}$ and HBC-$C_{14,10}$ in different phases (figures 1 and 2) reveal that the HBC-$C_{10,6}$ forms an ordered mesophase (smectic phase) at intermediate temperatures while the HBC-$C_{14,10}$ revealed the absence of any mesophase.

To identify the exact morphologies (and to compare with earlier published data [5]) of HBC-$C_{10,6}$ and HBC-$C_{14,10}$, we investigated the temperature-dependent 2D-WAXS patterns of macroscopically oriented samples (the same samples were subsequently used in the DS study). In the columnar plastic crystalline phase (figure 1) i.e. below the first transition (290 K), the distinct equatorial reflections suggest a well-ordered supramolecular structure. The off-meridional reflections indicate either (i) an identical tilt of the discotic cores with respect to the columnar axis with an intracolumnar period of 0.5 nm leading to a 'herringbone' structure (as anticipated from earlier studies) [5] or (ii) to the presence of a helical arrangement of discs. At 290 K, a considerable structural change occurred, accompanied by the fading of the meridional reflections (Col_d). On the other hand, a direct transition from the columnar plastic crystalline phase (Col_p) to the isotropic phase, without an intermediate LC phase, was observed in HBC-$C_{14,10}$ (figure 2). Thus the DSC, POM, and x-ray studies confirm the phase transformations. In addition, DSC revealed, for the first time, the presence of a glass temperature within the Col_p phase. The origin of the freezing of the dynamics at T_g within the Col_p phase can best be studied by dielectric spectroscopy.

3.2. Dynamics

The molecular dynamics of the HBC-$C_{10,6}$ and HBC-$C_{14,10}$ in the different phases (Col_p, Col_d and I) were investigated by DS. Surprisingly, the two compounds display a dipolar relaxation that is faster and more intense in the HBC-$C_{14,10}$ as compared to in HBC-$C_{10,6}$ (figure 3). The dielectric strengths

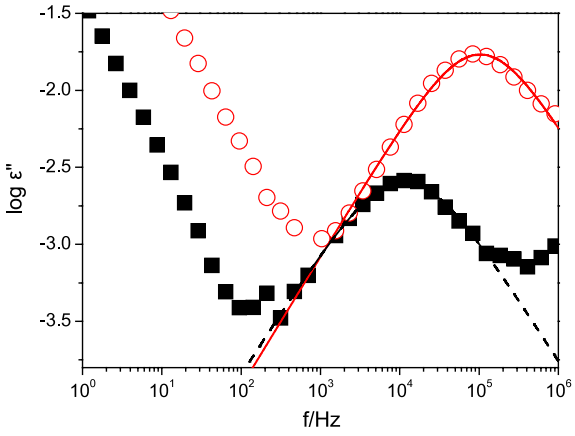

Figure 3. Comparison of the α-process of the HBC-$C_{10,6}$ (■) and HBC-$C_{14,10}$ (○) at 323.15 K. The solid and dashed lines are fits to the HN equation (see text).

of these processes are very weak ($T\Delta\varepsilon \sim 7$ K for HBC-$C_{10,6}$ and ~12 K for HBC-$C_{14,10}$) as compared to functionalized HBCs with strong dipole moments ($T\Delta\varepsilon \sim 217$ K for mono-cyano HBC) [31]. This process has a rate similar to the α-process found recently in the dipole-functionalized HBCs, thus is attributed to the in-plane disc rotation. The effective dipole moment ($\mu_{\text{eff}} = (g\mu)^{1/2}$, where μ is the dipole moment and g gives the orientation pair correlations between dipoles) responsible for the α process can be calculated from the dielectric strength using the Fröhlich equation applicable to spherically symmetric molecules [28]

$$\mu^2 = \frac{3\kappa_B T\Delta\varepsilon}{4\pi g N_0}\left(\frac{3}{\varepsilon_\infty + 2}\right)^2 \frac{2\varepsilon_0 + \varepsilon_\infty}{3\varepsilon_0} \qquad (4)$$

where $N_0 = \rho N_A/M_0$ is the number of dipoles per unit volume (ρ is the density, N_A is Avogadro's constant, k_B is the Boltzmann constant, M_0 is the molecular weight). As reported from earlier studies [32], the calculated densities of the HBCs are close to 1 g cm^{-3}. Using this macroscopic density in equation (4) gives $\mu_{\text{eff}} = 0.50\pm0.03$ and 0.60 ± 0.08 Debye for the HBC-$C_{10,6}$ and HBC-$C_{14,10}$, respectively. This dipole moment is very weak compared with the 4.55 ± 0.30 Debye found in mono-cyano substituted HBC [31]. Given the symmetric molecular core of the two compounds, the observation of a strongly dielectrically active process is, at first sight, a surprise. For this reason, controlled oxidation experiments have been made to gain a better understanding of the origin of this relaxation. In these experiments, different samples have been prepared following a variety of experimental conditions. A freshly prepared sample under argon atmosphere was measured by DS and has shown a very weak α-process. Then the same sample was heated to the isotropic phase for different time intervals and then measured by WAXS and DS. We found a stronger dielectric strength (DS) and at the same time, a better organized Col_p phase (WAXS). Clearly, oxidation promotes the π–π stacking of the aromatic cores, giving rise to a long-range orientation. Different samples prepared under similar conditions confirmed that the strength of the α-process varies with the degree of oxidation.

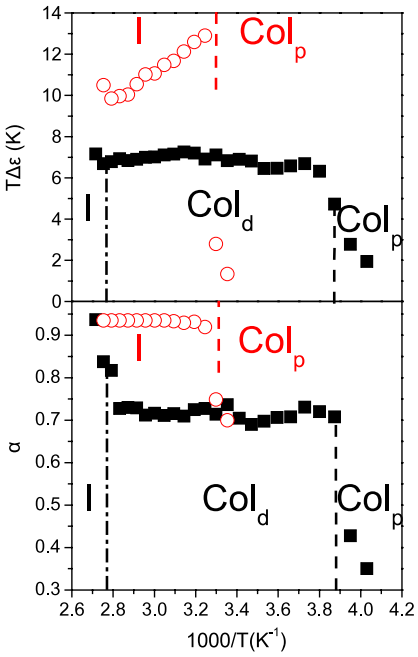

Figure 4. Top: T-dependence of the dielectric strength ($T\Delta\varepsilon$) corresponding to the α-process of the HBC-$C_{10,6}$ (■) and HBC-$C_{14,10}$ (○). The vertical dashed and dash–dotted lines give the locations of the transition temperatures from DSC on cooling, except the one for the HBC-$C_{10,6}$ from Col_p to Col_d phase which is obtained from DS on cooling. Bottom: T-dependence of the shape parameter (α) of the Havriliak–Negami (HN) function characterizing the distribution of relaxation times of the HBC-$C_{10,6}$ (■) and HBC-$C_{14,10}$ (○).

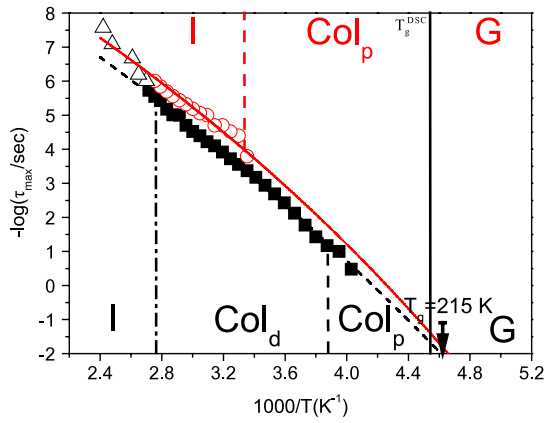

Figure 5. Arrhenius relaxation map for the HBC-$C_{10,6}$ (■) and HBC-$C_{14,10}$ (○). The solid and dashed lines are fits to the VFT equation (see text). The vertical lines correspond to the transition temperatures obtained from DSC on cooling except the one for the HBC-$C_{10,6}$ from Col_p to Col_d phase which is obtained from DS on cooling. NMR data (△) obtained from [33] of the core-deuterated molecule (HBC-C_{12}) is included for comparison.

The dielectric strength ($T\Delta\varepsilon$) as well as the distribution of relaxation times associated with the α-process are shown in figure 4. Remarkable changes in the dielectric strength and the shape parameters were found on entering the Col_p and Col_d phases. For the HBC-$C_{14,10}$ the dielectric strength dropped from $T\Delta\varepsilon \sim 12$ K in the I phase to 2 K on entering the Col_p phase. The symmetrical (α) and asymmetrical ($\alpha\gamma$) broadening parameters assumed values of $\alpha = \alpha\gamma = 0.94$ (in the isotropic phase) and $\alpha = \alpha\gamma = 0.7$ (in the Col_p phase). The broadening of the relaxation spectrum suggests increased cooperativity within the Col_p phase. On the other hand, for HBC-$C_{10,6}$ the shape parameters assumed values of $\alpha = \alpha\gamma = 0.94$ (in the I phase), $\alpha = \alpha\gamma = 0.7$ (in the Col_d phase) and $\alpha \sim \alpha\gamma \sim 0.4$ (in the Col_p phase). From the above is evident that the Col_p phase shows by far the more cooperative α-process.

The temperature-dependence of relaxation times, $\tau(T)$, is shown in figure 5 as a function of inverse temperature in the usual Arrhenius representation. The lines are fits to the well-known Vogel–Fulcher–Tammann (VFT) equation

$$\tau_{max} = \tau_0 \exp\left(\frac{B}{T - T_0}\right) \qquad (5)$$

where B is an activation parameter, T_0 is the 'ideal' glass temperature located near but below the T_g and τ_0 is the high temperature intercept. The VFT parameters τ_0, B and T_0 assumed values of 3×10^{-14} s, 5520 ± 440 K, and 62 ± 22 K for the HBC-$C_{10,6}$ and 3×10^{-14} s, 4800 ± 400 K, and 80 ± 14 K for the HBC-$C_{14,10}$. From the VFT dependence, the glass temperature can be estimated as the temperature where the corresponding α relaxation times are of the order of 10^2 s. The thus obtained glass temperatures are 217 ± 22 K and 215 ± 14 K for the HBC-$C_{10,6}$ and HBC-$C_{14,10}$, respectively, in excellent agreement with the values obtained from DSC. Interestingly, the $\tau(T)$ dependence is continuous throughout the transitions. This probably relates to the very weak dipole moment of the compounds. Nevertheless, we have shown the presence of a glass temperature in both HBCs. This could have consequences in the design of discotics with optimal charge carrier mobility. Previous NMR studies on a core-deuterated molecule revealed that the glass temperature is associated with a cooperative axial motion of the discs around the columnar axis [15]. To understand the geometry of the process seen in DS, NMR results on a core-deuterated HBC-C_{12} [33] are included in figure 5. The NMR data have an apparent activation energy of 114 kJ mol^{-1} and are in close proximity to the DS data, suggesting that both techniques are following the same process. This clearly demonstrates that the glass temperature of the two compounds is associated with cooperative axial rotational motion of the discs around the columnar axis. Thus, the T_g in HBCs corresponds to the freezing of the in-plane disc rotation at ∼215 K.

4. Conclusions

The two HBCs investigated by dynamic and structural probes revealed the presence of different columnar phases. Dielectric spectroscopy revealed a single cooperative VFT-like process freezing at ∼215 K, associated with the freezing of the in-plane disc rotation. Oxidation increases the dielectric strength of the process and promotes columnar stacking. Although the temperature-dependent relaxation times were continuous throughout the phase transformations, the broadening of

the relaxation spectra was discontinuous at the respective temperatures. Among the different ordered phases, the plastic crystalline phase (Col_p) possesses the highest cooperativity for the in-plane disc rotation.

Acknowledgments

M M Elmahdy is supported by a state fellowship (IKY). We are grateful to Professor H W Spiess for making available to us the NMR data on HBC-C_{12}. We thank Mr George Tsoumanis for technical support at the UoI.

References

[1] Boden N, Bushby R J, Clements J, Movaghar B, Donovan K J and Kreouzis T 1995 *Phys. Rev.* B **52** 13274
[2] Pisula W, Menon A, Stepputat M, Lieberwirth I, Kolb U, Tracz A, Sirringhaus H, Pakula T and Müllen K 2005 *Adv. Mater.* **17** 684
[3] van de Craats A M, Warman J M, Fechtenkötter A, Brand J D, Harbison M A and Müllen K 1999 *Adv. Mater.* **11** 1469
[4] Warman J M and van de Craats A M 2003 *Mol. Cryst. Liq. Cryst.* **396** 41
[5] Pisula W, Kastler M, Wasserfallen D, Mondeshki M, Piris J, Schnell I and Müllen K 2006 *Chem. Mater.* **18** 3634
[6] Stabel A, Herwig P, Müllen K and Rabe J P 1995 *Angew. Chem. Int. Edn* **34** 1609
[7] Wu J, Pisula W and Müllen K 2007 *Chem. Rev.* **107** 718
[8] Kastler M, Pisula W, Wasserfallen D, Pakula T and Müllen K 2005 *J. Am. Chem. Soc.* **127** 4286
[9] Fischbach I, Pakula T, Minkin P, Fechtenkötter A, Müllen K, Spiess H W and Saalwachter K 2002 *J. Phys. Chem.* B **106** 6408
[10] Möller M, Wendorff J H, Werth M and Spiess H W 1994 *J. Non-Cryst. Solids* **170** 295
[11] Möller M, Wendorff J H, Werth M, Spiess H W, Bengs H, Karthaus O and Ringsdorf H 1994 *Liq. Cryst.* **17** 381
[12] Groothues H, Kremer F, Collard D M and Lillya C P 1995 *Liq. Cryst.* **18** 117
[13] Kruglova O, Mendes E, Yildirim Z, Wübbenhorst M, Mulder F M, Stride J A, Picken S J and Kearley G J 2007 *ChemPhysChem* **8** 1338
[14] Yildirim Z, Wübbenhorst M, Mendes E, Picken S J, Paraschiv I, Marcelis A T M, Zuilhof H and Sudhölter E J R 2005 *J. Non-Cryst. Solids* **351** 2622
[15] Leisen J, Werth M, Boeffel C and Spiess H W 1992 *J. Chem. Phys.* **97** 3749
[16] Belushkin A V, Cook M J, Frezzato D, Haslam S D, Ferrarini A, Martin D, McMurdo J, Nordio P L, Richardson R M and Stafford A 1998 *Mol. Phys.* **93** 593
[17] Kearley G J, Mulder F M, Picken S J, Kouwer P H J and Stride J 2003 *Chem. Phys.* **292** 185
[18] Kruglova O, Mulder F M, Picken S J, Stride J and Kearley G J 2004 *Physica* B **350** e1003
[19] Andrienko D, Marcon V and Kremer K 2005 *J. Chem. Phys.* **125** 124902
[20] Glüsen B, Kettner A and Wendorff J H 1997 *Mol. Cryst. Liq. Cryst.* **303** 115
[21] Glüsen B, Kettner A, Kopitzke J and Wendorff J H 1998 *J. Non-Cryst. Solids* **241** 113
[22] Glüsen B, Heitz W, Kettner A and Wendorff J H 1996 *Liq. Cryst.* **20** 627
[23] Vallerien S U, Werth M, Kremer F and Spiess H W 1990 *Liq. Cryst.* **8** 889
[24] Werth M, Vallerien S U and Spiess H W 1991 *Liq. Cryst.* **10** 759
[25] Kastler M, Pisula W, Laquai F, Kumar A, Davis R, Baluschev S, Garcia-Gutiérrez M C, Wasserfallen D, Butt H J, Riekel C, Wegner G and Müllen K 2006 *Adv. Mater.* **18** 2255
[26] Pisula W, Kastler M, Wasserfallen D, Robertson J W F, Nolde F, Kohl C and Müllen K 2006 *Angew. Chem. Int. Edn* **45** 819
[27] Floudas G 2002 *Broadband Dielectric Spectroscopy* (New York: Springer)
[28] McCrum B G, Read B E and Williams G 1991 *Anelastic and Dielectric Effects in Polymeric Solids* (New York: Dover)
[29] Kumar S 2006 *Chem. Soc. Rev.* **35** 83
[30] de Gennes P G 1983 *J. Phys. Lett.* **44** 657
[31] Elmahdy M M, Floudas G, Mondeshki M, Spiess H W, Dou X and Müllen K 2008 *Phys. Rev. Lett.* **100** 107801
[32] Ito S, Wehmeier M, Brand J D, Kübel C, Epsch R, Rabe J P and Müllen K 2000 *Chem. Eur. J.* **6** 4327
[33] Kayser C W 1999 *PhD Thesis* Mainz